Archives of Acoustics Vol. 49, No. 1, pp. 107–120 (2024), doi: 10.24425/aoa.2024.148773

Research Paper

DOA Estimation of Ultrasonic Signal by Indirect Phase Shift Determination

Bogdan KRECZMER

Department of Cybernetics and Robotics, Faculty of Electronics, Photonics and Microsystems
Wrocław University of Science and Technology
Wrocław, Poland; e-mail: bogdan.kreczmer@pwr.edu.pl

(*received March 25, 2023; accepted October 4, 2023; published online January 17, 2024*)

The paper presents the concept of the method of determining the direction of ultrasonic signal arrival, i.e., the azimuth and elevation angles. This method is an extension of the previous approach which was proposed to determine only the azimuth angle. The approach is based on the indirect phase determination. This makes it possible to tolerate spacing of receivers greater than half the wavelength of the received signal. At the same time, it provides increased measurement accuracy and reduced hardware requirements. To check the robustness of the method, simulations were carried out for the geometric arrangement of the receivers of the sonar module, for which the method was then implemented. This sonar module was used in the conducted experiments. The results of these simulations and experiments are included in the paper and discussed.

Keywords: direction of arrival; signal phase; sonar; ultrasonic range finder.

1. Introduction

Determining the direction of arrival (DOA) for an ultrasonic signal is an essential issue for the effective use of ultrasonic echolocation in mobile robot navigation. However, this is not the only area of application of this type of sensors. A very important field where it is also possible to use such a device is in supporting the activities of people who are blind or visually impaired. In this case in particular, a very important requirement is, on the one hand, to reduce energy consumption and simplify calculations, and on the other hand, to increase the reliability of detection and perception of the environment. This problem is addressed in this paper. The proposed approach makes it possible to estimate the DOA using the indirect determination of the signal phase shift. Because it does not rely on a signal amplitude measurement, no sampling is needed and computations are simplified. Experimental verification of the method was carried out using a sonar module equipped with four convectional piezoelectric receivers.

The problem of determining DOA is an area of intensive research. There are many methods to deal with this problem. A brief overview of them is given in the next section. Then, in Sec. 3, the basic concept of the indirect phase determination method is presented. The problem that arises in the proposed method is the ambiguity of the solutions. This is described in Sec. 4. How the ambiguities can be removed is the subject of Sec. 5. Then, Sec. 6 discusses the robustness of the method. Computations of the limit of the tolerable measurement errors for a specific arrangement of receivers are presented in Sec. 7. This layout of receivers was applied to the sonar module used in the experiments. Section 8 presents an approach to reducing the impact of noise on DOA determination. The results of the experiments are described and discussed in Sec. 9. The conclusions and scope of future work are presented in the final section.

2. Determining direction of signal arrival

The simplest approaches to DOA estimation are based on triangulation methods. They rely on time-of-flight (TOF) measurements (Peremans *et al.*, 1993; Kleeman, 1995; Choi *et al.*, 2014). However, much more effective approaches use array signal processing. These are the most common techniques for determining DOA that find applications in radar, sonar, medicine or communications. Two categories of such approaches can be distinguished, namely spectral-

based and parametric (Krim, Viberg, 1996). Methods falling into the first of these categories include beamforming (Krishnaveni *et al.*, 2013) and the algorithm of multiple signal classification (MUSIC) (Schmidt, 1986), as well as its variants, i.e., the total spectral search MUSIC method (Zhou *et al.*, 2013), or the partial spectral search (Sun *et al.*, 2015). The second category includes methods such as deterministic maximum likelihood (DML) (Cadzow, 1990), root-MUSIC (Barabell, 1983) and the estimation of signal parameters via rotational invariance techniques (ESPRIT) (Roy *et al.*, 1986; Roy, Kailath, 1989). The latter method has several other variants and adaptations, e.g., Unitary ESPRIT (Haardt, Nossek, 1995), Conjugate ESPRIT (Tayem, Kwon, 2003).

The aforementioned methods require a large number of floating-point calculations. Beamforming allows for some simplifications. This technique acts as a spacial filter (Van Veen, Buckley, 1988). It includes delay-and-sum approaches and as well as other methods based on different weights of added signals that are delivered by individual receivers. Changes in the weight values make it possible to control sidelobes. However, even with uniform weights, good results can be obtained (Dokmanić, Tashev, 2014). The most important advantage of the delay-and-sum technique is that it can be implemented in hardware. Such implementations using MEMS microphones and FPGA are presented in (Kerstens *et al.*, 2017; 2019; Allevato *et al.*, 2020). Unfortunately, this does not allow for high angular resolution. Therefore, the improved version of the sensor presented in (Kerstens *et al.*, 2019), uses an implementation of the MUSIC algorithm (Verellen *et al.*, 2020). Such an approach provides much more accurate environmental data at the cost of increased computational complexity. To reduce this, methods based on co-prime arrays are proposed (Yang *et al.*, 2018; Li *et al.*, 2020). In this approach, a co-prime array is divided into two or more uniform sparse subarrays. In these subarrays, the distances between the receivers can be greater than half the wavelength of the received signal. This results in ambiguity in the determination of DOA for each subarray. However, they can be eliminated because the distances in each subarray are co-prime numbers. The similar idea can be found in (Gialich *et al.*, 2012). Instead of exploiting several subarrays with uniform spacing between receivers greater than half a wavelength, a single such receiving array is used in (Chen *et al.*, 2020). The problem of DOA ambiguity is solved by emitting pulses at different frequencies.

Despite described improvements, the discussed approaches involve methods that are relatively computationally expensive. Most of them are able to determine the DOA of signals that come from several sources. The approach presented in this paper is restricted to the problem of DOA determination for an echo coming from a single direction. This is the obvious drawback. However, when an emitted signal is short enough, it can be acceptable for many applications of mobile robot navigation. The important advantages are that the computational burden is reduced and the hardware requirements are very low. Despite this, the method allows for good DOA estimation accuracy. In this sense, the proposed approach can be exploited in order to build an inexpensive sonar that will be an attractive replacement of traditional ultrasonic range finders. Such an inexpensive device can also become a good support for the blind and visually impaired.

3. Indirect signal phase determination

To locate an object using ultrasonic sonar, in addition to measuring the distance to it, the key is to find the direction from which the echo of the reflected signal arrives. Using the horizontal coordinate system, DOA is determined by the azimuth and elevation angles denoted here as ϕ and θ, respectively (see Fig. 1). The problem of their determination can be simplified when considering a narrowband signal. This approach becomes natural when a piezoelectric transducer is used as an emitter. An important advantage of using piezoelectric over electrostatic transmitters is that their signal emission is actually limited to the ultrasonic band only. Electrostatic transducers during emission of ultrasonic wave, also emit quiet sizzles in the audible band. Despite the fact that they are not loud, when they are repeated very often they are annoying. This type of sizzling is also emitted by piezoelectric transducers. However, they are much quieter. In practice, they can be noted by a person when the transducer is no more than a few centimeters from the ear.

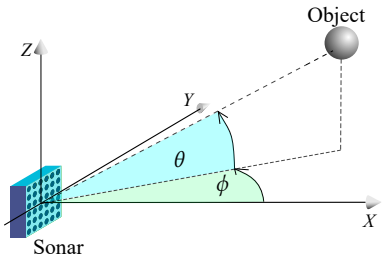

Fig. 1. Horizontal coordinates of an object in relation to a sonar.

Considering a narrowband signal, some simplifications can be made. It may be assumed that the signal carrier has a constant frequency. In fact, in the presented approach it is sufficient to assume that changes of signal carrier frequency are negligible during about three signal periods. Assuming that the signal source is in the far-field of the receivers, the signal wave can be treated as a plane wave. This is a common ap-

proach in signal array processing (Van Trees, 2004). Using these assumptions, a phase shift measurement can be applied to determine DOA. For the 1-D case, when only one angle is being determined, e.g., the azimuth angle, it is sufficient to use two receivers provided that their mutual distance is less than half the signal wavelength. For the 2-D case, when two angles are determined, i.e., the azimuth and elevation angles, three receivers are needed, which must be placed non-collinearly and must be two pairs whose mutual distances are lower than half the signal wavelength. Since a plane wave can be modeled as a set of planes relating to specific signal phases, wave points belonging to the same signal phase must satisfy the equation:

$$\mathsf{a}x + \mathsf{b}y + \mathsf{c}z + \mathsf{d} = 0, \tag{1}$$

where a, b, and c are coordinates of the vector perpendicular to the plane. Considering a plane wave, it is convenient to use a normalized vector pointed to the direction of wave propagation expressed by direction cosines, i.e.:

$$\boldsymbol{a} = \begin{bmatrix} -\cos\theta\cos\phi \\ -\cos\theta\sin\phi \\ -\sin\theta \end{bmatrix}. \tag{2}$$

Thus, Eq. (1) can be rewritten as

$$a_x x + a_y y + a_z z + \mathsf{d} = 0, \tag{3}$$

where $\boldsymbol{a} = (a_x, a_y, a_z)$. When a plane wave is propagated towards the origin of the coordinate system, then d is the distance of the plane wave from the origin. For a plane wave propagated in the opposite direction, d has the same absolute value, but with the minus sign. Equation (3) is a special form of a more general function:

$$D(\boldsymbol{p}) = a_x x_p + a_y y_p + a_z z_p + \mathsf{d}, \tag{4}$$

where $\boldsymbol{p} = (x_p, y_p, z_p)$. The absolute value of this function for a point $\boldsymbol{p}$ corresponds to its distance to the plane described by Eq. (3). The sign of this value depends on which side of the plane the point $\boldsymbol{p}$ is located.

Considering the set of three receivers, it is useful to choose such a coordinate system that its origin is at the center of one of them, e.g., the receiver R_0 (see Fig. 2). For the sake of simplicity, let us assume that the signal wavefront first reaches the receiver R_0 (this assumption will be dropped later). Then, the wavefront is detected by receivers R_1 and R_2. The data obtained allow expressing the distances from receivers R_1 and R_2 to the plane wave (see Fig. 3a) as follows:

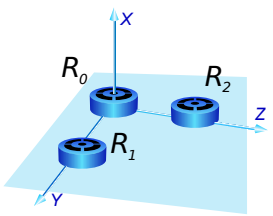

Fig. 2. Coordinate system for the set of three receivers.

$$s_1 = v_a\tau_{01}, \qquad s_2 = v_a\tau_{02}, \tag{5}$$

where v_a is the speed of the acoustic wave, $\tau_{01} = t_1 - t_0$, $\tau_{02} = t_2 - t_0$ and t_0, t_1, t_2 are the wave detection times by receivers R_0, R_1, and R_2, respectively. On the other hand, these distances can be determined using the function $D(.)$ modeling a plane wave corresponding to the moment of arrival at the receiver R_0. It gives

$$D(R_1) = s_1, \qquad D(R_2) = s_2.$$

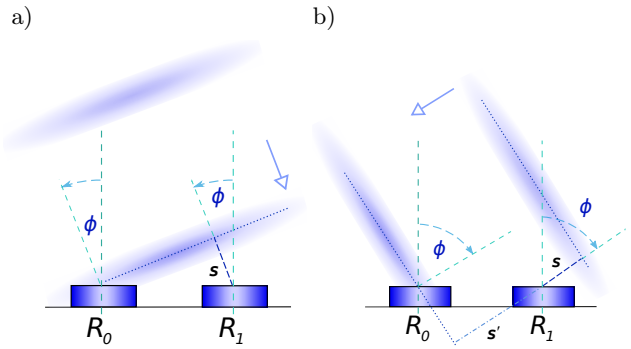

Fig. 3. Distance to the wavefront when the receiver R_0 is reached: a) before R_1; b) after R_1.

Since the plane wave at that moment contains the origin of the coordinate system, then $\mathsf{d} = 0$. Taking into account that $R_1 = (0, y_1, z_1)$ and $R_2 = (0, y_2, z_2)$ and the the vector $\boldsymbol{a}$ is normalized, a system of equations is obtained:

$$\begin{cases} a_y y_1 + a_z z_1 = s_1, \\ a_y y_2 + a_z z_2 = s_2, \\ a_x^2 + a_y^2 + a_z^2 = 1. \end{cases} \tag{6}$$

Its solution is

$$\begin{aligned} a_y &= \frac{z_2 s_1 - z_1 s_2}{y_1 z_2 - y_2 z_1}, \\ a_z &= \frac{y_1 s_2 - y_2 s_1}{y_1 z_2 - y_2 z_1}, \\ a_x &= \sqrt{1 - a_y^2 - a_z^2}. \end{aligned} \tag{7}$$

According to Eq. (2)

$$a_z = -\sin\theta \quad \wedge \quad a_y = -\cos\theta\sin\phi. \tag{8}$$

Due to the fact that $\theta \in \left(-\frac{\pi}{2}, \frac{\pi}{2}\right)$, its cosine values are positive. As a result, the expression of a_y can be rewritten to the form:

$$a_y = -\left(\sqrt{1 - a_z^2}\right)\sin\phi.$$

This gives the formulas for calculating the azimuth and elevation angles:

$$\phi = \arcsin -\frac{a_y}{\sqrt{1-a_z^2}}, \qquad \theta = \arcsin -a_z. \tag{9}$$

They show that a_x does not need to be computed to find ϕ and θ.

The presented calculation procedure can be directly applied to the obtained measurements when the distance between the receivers is not more than half the wavelength of the received signal, and the same wavefront is detected first by the receiver R_0 and then by R_1. In such a case, the signal detection times t_0 and t_1 satisfy the relationship:

$$0 \le t_1 - t_0 < \frac{T_a}{2}.$$

Otherwise, when after registering the first wavefront by R_0, R_1 registers the next wavefront (see Fig. 3b), the following condition is fulfilled:

$$\frac{T_a}{2} \le t_1 - t_0 < T_a.$$

These conditions are disjoint because the distance between the receivers is assumed to be less than half the wavelength. In the last case discussed, a correction is needed to calculate the correct distance s' (see Fig. 3b), namely:

$$\tau'_{01} = t_1 - t_0 - T_a. \tag{10}$$

In this case, $s' < 0$ which means that R_1 is behind the wavefront detected by R_0 (see Fig. 3b).

4. Ambiguities for larger mutual distances of receivers

Using popular piezoelectric transducers as receivers, it is impossible to meet the condition that their mutual distances are less than half the wavelength. This is because their smallest diameter is about 10 mm. Fortunately, there are available MEMS microphones on the market, which have much smaller housing and allow the mutual distances to be reduced. Sensor constructions which exploit them to create microphone arrays are presented in (Steckel *et al.*, 2013; Verellen *et al.*, 2020). Nevertheless, it is still useful to have longer mutual distances as this can reduce the error in determining the azimuth and elevation angles. In (Kreczmer, 2018), it was shown that such a result is obtained for 2-D sonar (i.e., determining distance and azimuth angle) for calculating the azimuth angle values. However, when mutual distances between receivers are greater than half the wavelength of the signal, ambiguities arise. This is due to the fact that the same distances s_1 and s_2 refer to several DOAs. As discussed before, when the plane wave detected by R_0 is not the same one detected by R_1 or R_2, a correction should be added to the measured time τ_{01} or τ_{02}, respectively. This correction is a multiple of the signal period T_a. It can be different for both receivers. Equation (10) is a special case of such a correction for which the multiplier equals −1.

The possible measurement values of τ_{0i} (where $i \in \{1,2\}$) are determined by the distance between receivers R_0 and R_i. Since for a given τ_{0i}, only the relative position of the two respective receivers need be considered, the range of possible multiples for the full range of arrival angles $\boldsymbol{\alpha} = \left[-\frac{\pi}{2}, \frac{\pi}{2}\right]$ is limited to:

$$\mathcal{I}_{\boldsymbol{\alpha}}(b_{0i}) = \left\{k : k \in \boldsymbol{I} \ \wedge \ \left\lfloor -\frac{b_{0i}}{\lambda} \right\rfloor \le k \le \left\lfloor \frac{b_{0i}}{\lambda} \right\rfloor\right\},$$

where $i \in \{1,2\}$ and the range of variation of indices in further expressions, in this section, is the same, $\boldsymbol{I}$ is the set of integer numbers, b_{0i} is the distance between R_0 and R_i, λ is the wavelength of the signal, and $\lfloor . \rfloor$ is the floor function. Due to the directionality of the receivers and transmitter, the range of signal arrival angles that can be detected is much smaller, i.e., $\boldsymbol{\alpha} = [\alpha_{\min}, \alpha_{\max}] \subset \left[-\frac{\pi}{2}, \frac{\pi}{2}\right]$. For simplicity, it can be assumed that the receivers have axial symmetry along their acoustic axes and have the same directivity pattern. Therefore, $\alpha_{\min} = -\alpha_{\max}$ and $\alpha_{\max} > 0$. Then, the range of possible multiples can be expressed as follows

$$\mathcal{I}_{\boldsymbol{\alpha}}(b_{0i}) = \left\{k : k \in \boldsymbol{I} \ \wedge \ \left\lfloor -\frac{b_{0i}\sin\alpha_{\max}}{\lambda} \right\rfloor \le k \le \left\lfloor \frac{b_{0i}\sin\alpha_{\max}}{\lambda} \right\rfloor\right\}.$$

Having a set of all multipliers, the set of possible values of time measurements can be constructed as follows:

$$\boldsymbol{\tau}_{\boldsymbol{\alpha}}(\tau_{0i}) = \{\tau_j : \tau_j = \tau_{0i} + kT_a, k \in \mathcal{I}_{\boldsymbol{\alpha}}(b_{0i}) \wedge |v_a\tau_j| < b_{0i}\}.$$

These times refer to the different possible directions of arrival of the wavefront detected by R_0, then R_1 or R_2. The times of signal detection by both receivers are related values. Their set can be defined as follows:

$$\boldsymbol{\tau}^2_{\boldsymbol{\alpha}}(\tau_{01}, \tau_{02}) = \{(\tau_i, \tau_j) : \tau_i \in \boldsymbol{\tau}_{\boldsymbol{\alpha}}(\tau_{01}) \wedge \tau_j \in \boldsymbol{\tau}_{\boldsymbol{\alpha}}(\tau_{02})\}.$$

Taking into account the velocity of the acoustic wave, a set of possible distances (s_i, s_j) to the wavefront can be created:

$$\boldsymbol{s}^2(\tau_{01}, \tau_{02}) = \{(s_i, s_j) : s_i = v_a\tau_i, s_j = v_a\tau_j, (\tau_i, \tau_j) \in \boldsymbol{\tau}^2_{\boldsymbol{\alpha}}(\tau_{01}, \tau_{02})\}.$$

Applying these distances to Eq. (6), the set of its solutions is obtained:

$$\mathfrak{a}^*(\tau_{01}, \tau_{02}) = \{(a_{x,1}, a_{y,1}, a_{z,1}), ..., (a_{x,k}, a_{y,k}, a_{z,k})\}.$$

Values of intervals τ_{01} and τ_{02} depend on geometry of the receiving system $\mathbb{R} = (R_0, R_1, R_2)$ and the received

signal S. Therefore, it is more convenient to use $\mathbb{R}$ and S as arguments of $\mathfrak{a}^\star$. It is also worth to note that it is enough to know a_y and a_z to calculate angles ϕ and θ. This makes it possible to consider a bit more restricted set defined as follows:

$$\mathfrak{a}^\star(\mathbb{R}, S) = \{(a_{y,1}, a_{z,1}), ..., (a_{y,k}, a_{z,k})\}.$$

This set of solutions determines all possible values of ϕ and θ for given measurements.

5. Ambiguity removal

It can be easily shown for the 1-D case of DOA that when mutual distances between receivers are properly chosen then the only common direction in the set of determined possible arrival angles, is the proper one (Kreczmer, 2019) (see Fig. 4). The same idea can be applied to the 2-D case of DOA. The main difference is that an elementary receiving system in the 2-D case has to consist of three receivers instead of two. In Fig. 5a, there is an arrangement of two such elementary systems $\mathbb{R}_a = (R_0, R_1, R_2)$ and $\mathbb{R}_b = (R_3, R_4, R_5)$. Applying the aforementioned idea, the solution sought is

$$\mathfrak{a}^\star(\mathbb{R}_a, S) \cap \mathfrak{a}^\star(\mathbb{R}_b, S).$$

These two systems can be integrated into one set in such a way that both have two common receivers

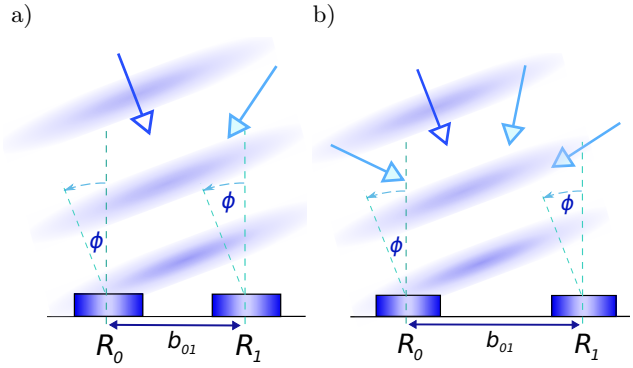

Fig. 4. Examples of possible incident angles for measurement data obtained while the real incident angle is equal to 20°. Directions were determined for the gap size b equal to: a) 11 mm; b) 15 mm.

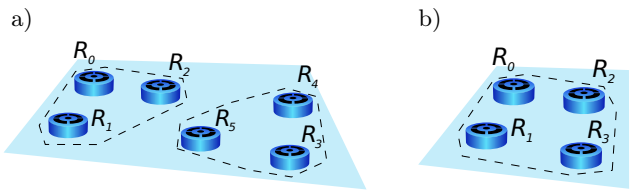

Fig. 5. Receiving system for the 2-D case that makes possible to solve the problem of ambiguity: a) two separate elementary receiving systems; b) a single integrated receiving system.

(see Fig. 5b). In this way, having the set of transducers $\boldsymbol{R} = (R_0, R_1, R_2, R_3)$, two receiving systems can be distinguished, i.e. $\mathbb{R}_1 = (R_0, R_1, R_2)$ and $\mathbb{R}_2 = (R_1, R_2, R_3)$. However, it is simple to notice, that also two additional systems can be found. In this case, they are $\mathbb{R}_3 = (R_0, R_1, R_3)$ and $\mathbb{R}_4 = (R_0, R_2, R_3)$. Taking into account all elementary systems, the solution sought is

$$\mathfrak{a}^\star(\mathbb{R}_1, S) \cap \mathfrak{a}^\star(\mathbb{R}_2, S) \cap \mathfrak{a}^\star(\mathbb{R}_3, S) \cap \mathfrak{a}^\star(\mathbb{R}_4, S).$$

6. Robustness

Due to the time measurement errors, the determined values of a_y and a_z are also burdened with them. It is convenient to assume that measurement errors of τ intervals are approximated by the same value $\Delta\tau$. Then, taking into account Eq. (7), errors in determining a_y and a_z can be estimated by formulas:

$$\begin{aligned} \Delta a_y &= \frac{|z_1| + |z_2|}{|y_1 z_2 - y_2 z_1|} v_a \Delta\tau, \\ \Delta a_z &= \frac{|y_2| + |y_1|}{|y_1 z_2 - y_2 z_1|} v_a \Delta\tau. \end{aligned} \tag{11}$$

They show that for each receiving system $\mathbb{R}_q$ the errors of determining the coordinates a_y and a_z are constant and strongly depend on the location of its receivers. Moreover, it is worth noting that to minimize Δa_y and Δa_z, the receivers R_1 and R_2 should be located along perpendicular lines crossing at the location of the receiver R_0. Following this idea and considering the arrangement of the receivers $R_1 = (0, y_1, 0)$ and $R_2 = (0, 0, z_2)$, Eq. (11) reduces to the form:

$$\Delta a_y = \frac{1}{|y_1|} v_a \Delta\tau, \qquad \Delta a_z = \frac{1}{|z_2|} v_a \Delta\tau. \tag{12}$$

6.1. Influence of measurement errors on the ambiguity of solutions

In order to take into account measurement errors, instead of a point set $\mathfrak{a}^2(\mathbb{R}_k, S)$, a set of rectangles is obtained. It can be defined as follows:

$$\begin{aligned} \mathfrak{a}^2_\Delta(\mathbb{R}_k, S) = \{ & A^i_{S,k} = [a_{y,i} - \Delta_k a_y, a_{y,i} + \Delta_k a_y] \\ & \times [a_{z,i} - \Delta_k a_z, a_{z,i} + \Delta_k a_z] : (a_{y,i}, a_{z,i}) \\ & \in \mathfrak{a}^2(\mathbb{R}_k, S)\}, \end{aligned}$$

where the index k identifies an elementary receiving system.

Assuming that the direction vector of propagation of the signal S is $\boldsymbol{a}_S = (a_{y,S}, a_{z,S})$, the uncertainty rectangle corresponding to the geometry of the system $\mathbb{R}_k$ and relating to the actual signal S is

$$\begin{aligned} A_{S,k} = & [a_{y,S} - \Delta_k a_y, a_{y,S} + \Delta_k a_y] \\ & \times [a_{z,S} - \Delta_k a_z, a_{z,S} + \Delta_k a_z]. \end{aligned}$$

According to the idea shown in Fig. 4, each receiving system determines the correct direction as one of possible solutions. Therefore, considering the set of receiving systems $\mathbb{R}^* = \{\mathbb{R}_1, \ldots, \mathbb{R}_m\}$, the uncertainty rectangles $A_{S,k}$ referring to subsequent receiving systems $\mathbb{R}_k$ must meet the condition:

$$\boldsymbol{a}_S \in \bigcap_{k=1}^{m} A_{S,k}. \tag{13}$$

The ambiguity is removed when there is only one sequence of uncertainty rectangles $A_{S,1}, ..., A_{S,m}$, denoted as $\boldsymbol{A}^*_S$, that creates a non-empty common part, i.e.:

$$\boldsymbol{a}_S \in \bigcap_{A_{S,k} \in \boldsymbol{A}^*_S} A_{S,k} \quad \wedge \quad \forall (A^j_{S,1}, ..., A^j_{S,m}) \neq \boldsymbol{A}^*_S, \quad \bigcap_{k=1}^{m} A^j_{S,k} = \varnothing. \tag{14}$$

In order to be able in a simple way to select the common part of all uncertainty rectangles, it is essential to choose the same orientation for the local coordinate frames of all elementary receiving systems.

6.2. Computing the angles of azimuth and elevation

When the results of measurements are not corrupted by any errors, the uncertainty rectangles meeting Eq. (13) have their centers in the common point $\boldsymbol{a}_S$ (see Fig. 6a). In the case of actual measurement values, the centers of the uncertainty rectangles are in different places due to errors. For correctly estimated values of measurement errors, all rectangles should contain a point corresponding to the coordinates of the actual signal direction (see Fig. 6b). There are several ways to estimate the coordinates of the true signal direction $\boldsymbol{a}_S$. To describe them a bit more formally, a function which extracts the coordinates of the middle point of the rectangle, denoted as $M(.)$, is used.

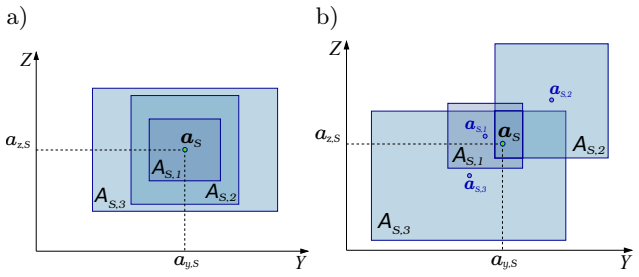

Fig. 6. Uncertainty rectangles satisfying Eq. (13) for the set of receiving systems $\mathbb{R}^* = \{\mathbb{R}_1, \mathbb{R}_2, \mathbb{R}_3\}$ and their measurements that: a) are not affected by errors; b) are affected by errors.

The simplest way is to calculate the mean values of the coordinates of the centers of the rectangles:

$$(\overline{a}_y, \overline{a}_z)_1 = \frac{1}{m} \sum_{i=1}^{m} M(A_{S,i}).$$

In order to distinguish the discussed approaches, a numerical index was provided along with the coordinates of the signal direction.

Using the more sophisticated approach, the uncertainty of the measured values are taken into account. The sizes of rectangles reflect the uncertainty of these values. The smaller the size, the more accurate the determination of the coordinates of the signal direction vector.

Denoting $L_y(.)$ and $L_z(.)$ as functions extracting the length of the uncertainty rectangle along the coordinate axes OY and OZ, respectively, the certainty coefficient for each coordinate can be expressed as follows:

$$C_y(A_{S,l}) = \frac{1}{L_y(A_{S,l})} \left(\sum_{k=1}^{m} \frac{1}{L_y(A_{S,k})} \right)^{-1},$$

$$C_z(A_{S,l}) = \frac{1}{L_z(A_{S,l})} \left(\sum_{k=1}^{m} \frac{1}{L_z(A_{S,k})} \right)^{-1}.$$

Then, the estimated coordinates can be computed using the formula

$$(\overline{a}_y, \overline{a}_z)_2 = \sum_{k=1}^{m} \big(C_y(A_{S,k}) M_y(A_{S,k}),\, C_z(A_{S,k}) M_z(A_{S,k}) \big),$$

where $M_y(.)$ and $M_z(.)$ extract the y and z coordinates of the center of the uncertainty rectangles $A_{S,k}$, respectively.

However, the most simple and very natural way is to calculate the coordinates of the center of the rectangle, that is the common part of them all:

$$(\overline{a}_y, \overline{a}_z)_3 = M \left(\bigcap_{i=k}^{m} A_{S,k} \right).$$

Having the coordinates $(\overline{a}_y, \overline{a}_z)$, the azimuth and elevation angles can be computed using Eq. (9). The effectiveness of the presented three approaches to DOA estimation is discussed in the next section.

7. Simulations

To find the range of tolerable measurement errors, computations were made for the azimuth and elevation angles using the signal detection times burdened with all possible combinations of measurement errors in a given range. The step of changing the time measurement error was $2^{-5} = 0.03125$ µs. The power of 2 was applied to eliminate the problem that results in the accumulation of calculation errors due to the finite representation of numbers. The value of time error Δt was increased until the value of the azimuth or elevation angle determined by the method no. 2 discussed in Subsec. 6.2 was greater than 10°. This procedure was also stopped when a combination of errors made

it impossible to remove the ambiguity of the DOA solution. In this way, the maximum value of the simulated time error for which the two conditions aforementioned were met was taken as the limit of the tolerable time measurement errors. The computations were performed for the geometrical arrangement of receivers presented in Fig. 7. It corresponds to the geometry of the sonar module used in experiments presented in Sec. 9. It was assumed that the sensitivity range of the receivers was $[-40°, 40°]$ in each direction. The results of the computations are presented in Fig. 8. The biggest found value of Δt is 1.91 µs. The diagram presented in Fig. 8 does not have any plane symmetry, due to unsymmetrical arrangement of receivers. However, it has the axial symmetry induced by the axis of Δt. This is due to the symmetry of the sine function used in Eq. (9).

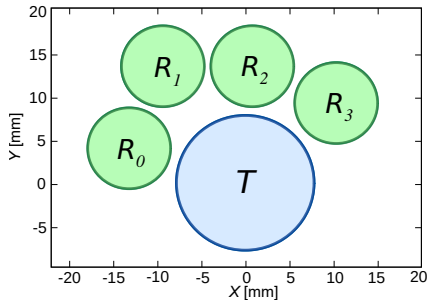

Fig. 7. Geometrical arrangement of sonar receivers and a transmitter.

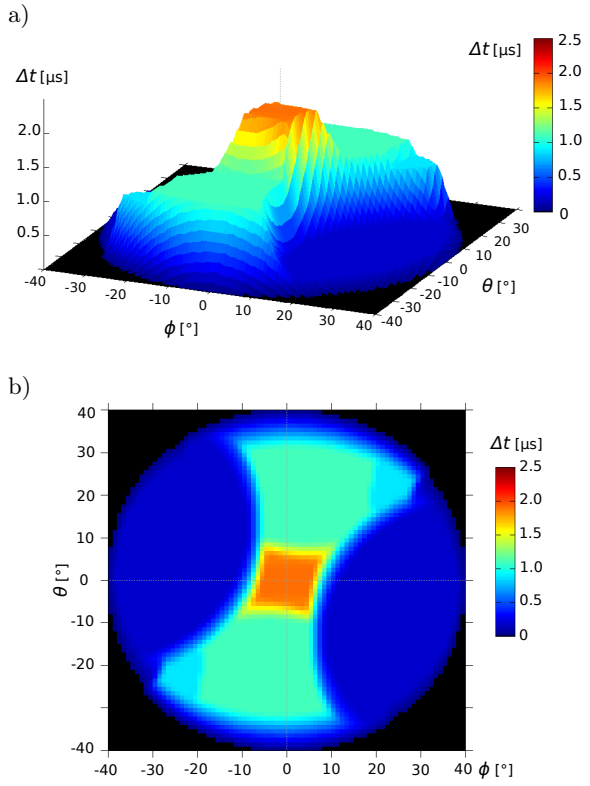

Fig. 8. Distribution of the maximal tolerable error of time measurement: a) side and b) top view.

In Subsec. 6.2, it was discussed how $\boldsymbol{a}_S$ can be estimated. The question then arises, using the same timing errors, which of the three approaches presented gives the best estimate of the angles ϕ and θ. Figure 9a shows a diagram comparing the maximum errors of azimuth angle estimation using the discussed approaches at $\theta = 0°$.

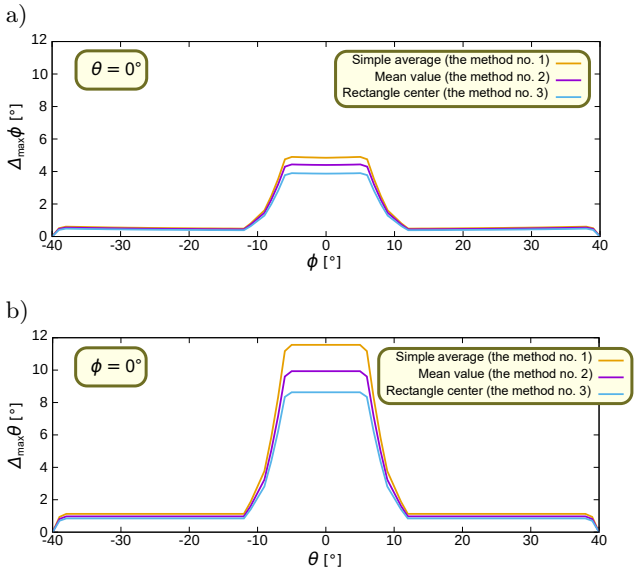

Fig. 9. The maximal errors for angles determined by the method no. 1, 2, and 3: a) for the azimuth angle at $\theta = 0°$; b) for the elevation angle at $\phi = 0°$.

An analogous diagram for the elevation angle at $\phi = 0°$, is presented in Fig. 9b. The mutual relation between errors in determining the angles ϕ and θ, visible in the diagrams, is also preserved for other directions. It was expected that the method no. 2 which involves some measure of uncertainty should be the best, but it is not. The best one is the method no. 3. An additional advantage of this situation is that this method is the simplest to compute. The same relation is also observed when comparing RMSD values.

It is worth noting that the error values for determining the elevation angle are much larger compared to the same type of errors for the azimuth angle (see Fig. 9). The increase in the error value is a direct consequence of the fact that the distance between the extreme receivers in the vertical plane is much smaller than their counterparts in the horizontal plane.

8. Reducing the impact of noise

The procedure described in the previous sections is applied to a single wavefront. However, it can also be applied to each successive one in a given wave packet, and then average values can be calculated. To explain this, the measurement procedure used in this method is presented in more detail. In order to detect a wave packet, the threshold method is used. It is worth em-

phasizing that this method is used only for detection, not for actual measurements, the results of which are used to determine DOA. When the signal in the receiver channels exceeds the detection threshold, in the next moment in each of these channels, the times of crossing the zero level are recorded (see Fig. 10a). Signal transitions through the zero level are detected only for raising edges. The results of these measurements do not depend on the value of the signal amplitudes. The measured times are used to determine the azimuth and elevation angles of DOA. Once a wave packet is detected, the same time measurements can be also performed for successive signal transitions through the zero level (see Fig. 10b). When the signal is reflected from a single object and there is no noise, the same angle values are obtained for all subsequent measurements. In the proposed approach, in order to reduce the influence of noise, averages of azimuth and elevation angles are calculated based on four consecutive wavefronts, whereby a measurement that deviates most from all others is discarded. This procedure starts with the third detected wavefront.

a)

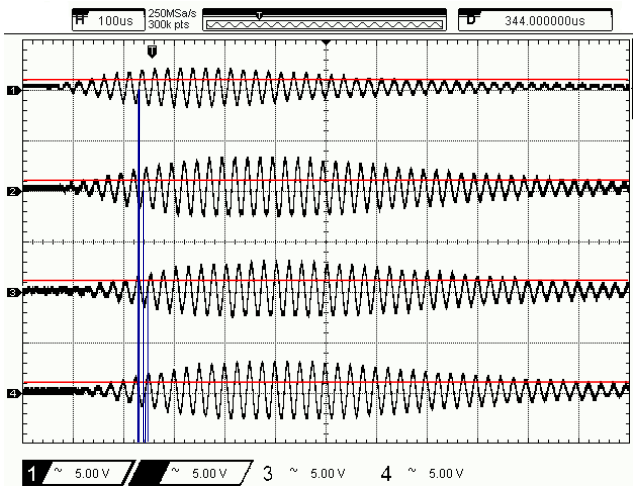

b)

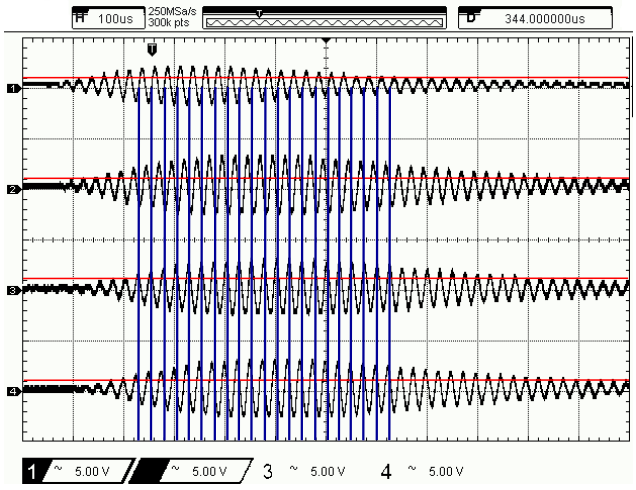

Fig. 10. Measurements of times of signal zero crossings: a) for a single signal pulse; b) for subsequent pulses for the entire wave packet, for clarity, moments of zero-crossing detection for the first receiver was marked only.

9. Experiments

In order to verify the effectiveness of the proposed method, a series of experiments was carried out using the sonar module shown in Fig. 11. This module consists of one BPU-1640IOAH12 transmitter and four MA40S4R receivers. All ultrasonic transducers are controlled by the mini-module (Cholewiński *et al.*, 2013), which exploits the microcontroller MK40DN512VLK10. To verify DOA determination for different orientations of the ultrasonic transducers, the sonar module was mounted on a rotating base. This made it possible to perform a scan in the horizontal plane with a step equal to 1°. Each scan was made in the angular range from −40° to 40°. It was taken 20 measurements for each orientation of the sonar module. This allowed the calculation of mean and RMSD values. The sonar module was placed 1.4 m above the floor. This made it possible to avoid the ground effect (Kapoor *et al.*, 2018). Measurements were made for two different cases. The first case was a series of measurements to a wall (see Fig. 13a). The second case was a series of measurements to a small glass ball suspended above the floor at different heights. For each case, the azimuth and elevation angles, i.e., ϕ and θ, were determined in the local coordinate system of the sonar module. To check the correctness of the calculation of the azimuth angle ϕ, its value was compared with the value of the orientation angle of the sonar module α, which was measured in the global coordinate system of the sonar stand. Considering the case of a wall, it can be noticed that echoes always arrive from the direction perpendicular to the wall surface and it does not depend on the sonar module orientation, if that direction is within the range of the sonar beam (see Fig. 12). Therefore, for the ideal case when there are no measurement errors, the relation between ϕ and α is as follows:

$$\phi = -\alpha. \tag{15}$$

A more detailed explanation of this feature can be found in (Kreczmer, 2019). The same relation is also

Fig. 11. Sonar module used in experiments.

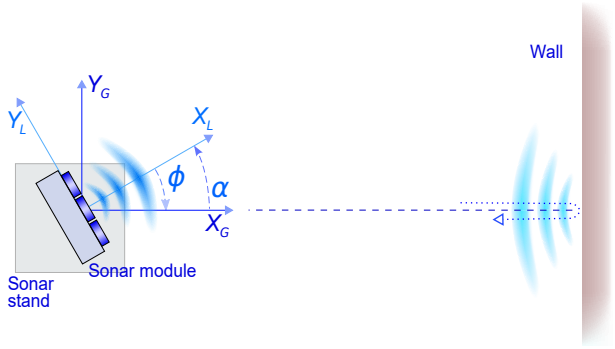

Fig. 12. Coordinate systems chosen for the experiment. The azimuth angle ϕ measured in the local coordinate system of the sonar module has an opposite sign to the rotation angle α measured in the global coordinate system.

valid for such an object as a glass ball used in these experiments. Performing measurements for the case of a wall, the sonar module was placed at a distance of about 2.4 m from the wall (see Fig. 13a). Over the entire range of sonar module orientations, the wall was detected, as shown in the diagram of distance measurements (see Fig. 13b). In the discussed experiments, the distance is measured by using the threshold detection method. Therefore, this type of measurements cannot be expected to be very accurate. Nevertheless, they show very well the orientation ranges of the sonar module for which an object was observed. Despite object detection over the entire range, DOA angles were determined properly in a smaller region, which is about $[-28°, 33°]$ (see Figs. 13c and 13d). This limitation results mainly from the directional characteristics of the transmitter, which emits a significantly weaker signal for directions well away from its acoustic axis.

According to the results of the simulations, it would be expected that the accuracy and precision of determining the azimuth angle would be higher than that of the elevation angle. However, this is not the case here. The diagram in Fig 14a shows the absolute values of the differences between the actual and determined values of the elevation and azimuth angles denoted as $\Delta\phi$ and $\Delta\theta$, respectively. It can be noticed that the discrepancies for both angles are similar. An analogous relationship is also observed for RMSD (see Fig. 14b). The reason is that the wall is a very good reflector and the returning echoes are strong. This results in small measurement errors. Their consequence is the small differences mentioned earlier.

The second series of experiments was done for the glass ball, which scatters the signal much more than the wall. In the first experiment of this series, the glass ball was placed at a distance of about 1.6 m from the sonar module and 1.8 m above the floor (see Fig. 15a). Due to the much weaker echo, SNR is decreased, and thus azimuth and elevation angles were determined correctly over a much smaller range of sonar module orientation (see Figs. 15b–d). This also results in

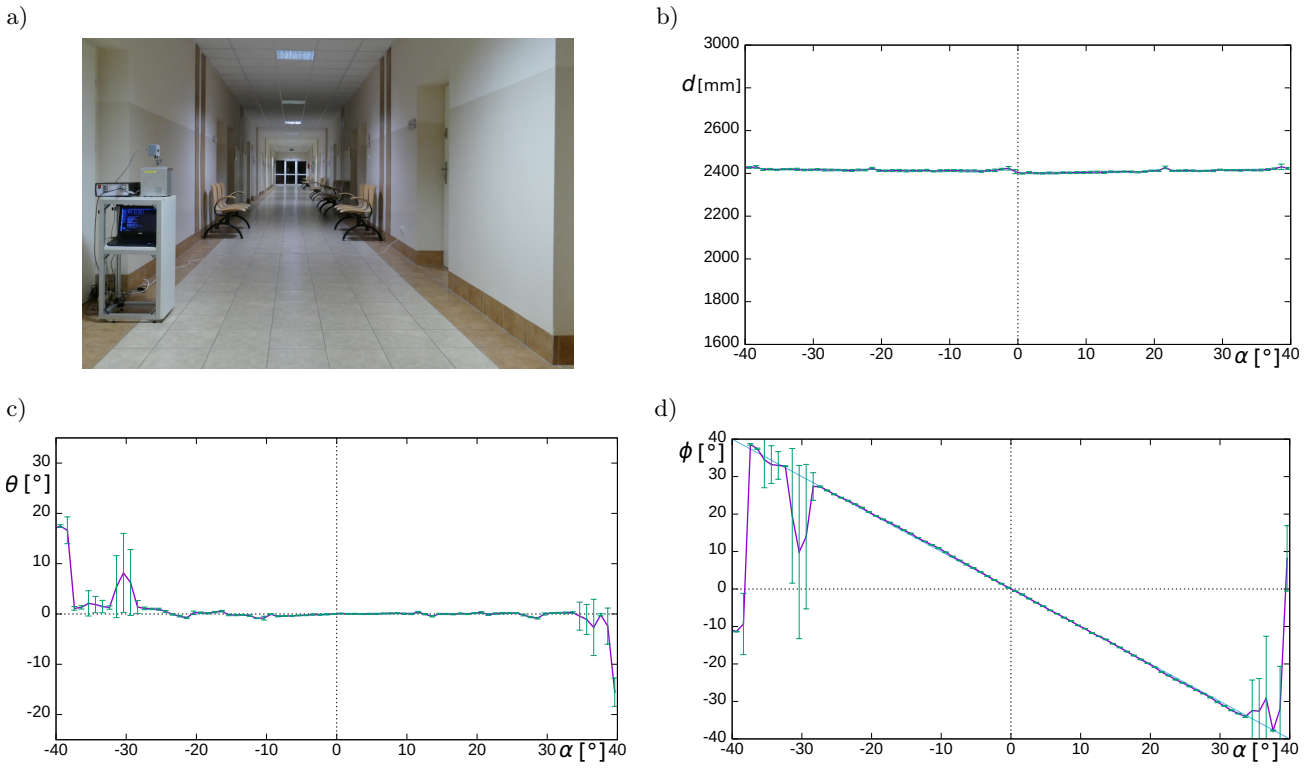

Fig. 13. Results of measurements performed for the wall depending on the orientation angle α of the sonar module, which was located at a distance of 2.4 m from the wall: a) arrangement of the sonar stand and the wall; b) values of the measured distance d; c) determined values of the elevation angle θ; d) determined values of the azimuth angle ϕ.

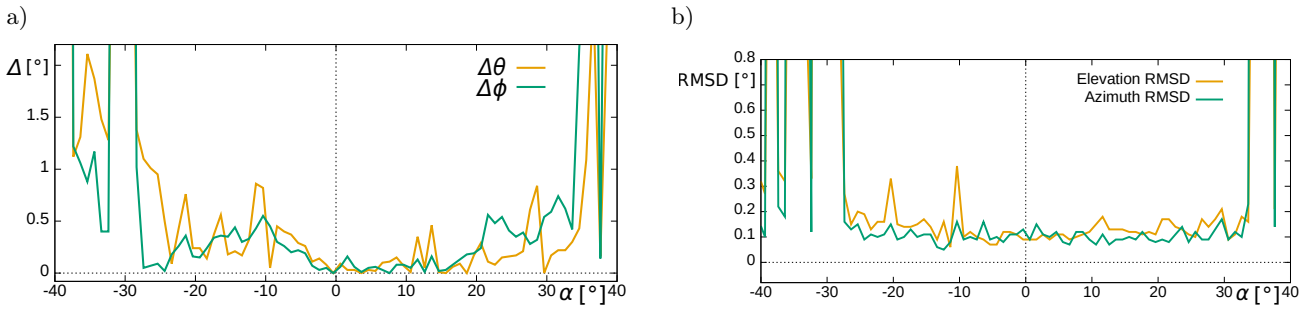

Fig. 14. Accuracy and precision of the azimuth and evaluation angles depending on the orientation angle α of the sonar module: a) accuracy expressed as the absolute value of the difference between the actual and determined values of the angles; b) precision expressed by RMSD of the determined values of the angles.

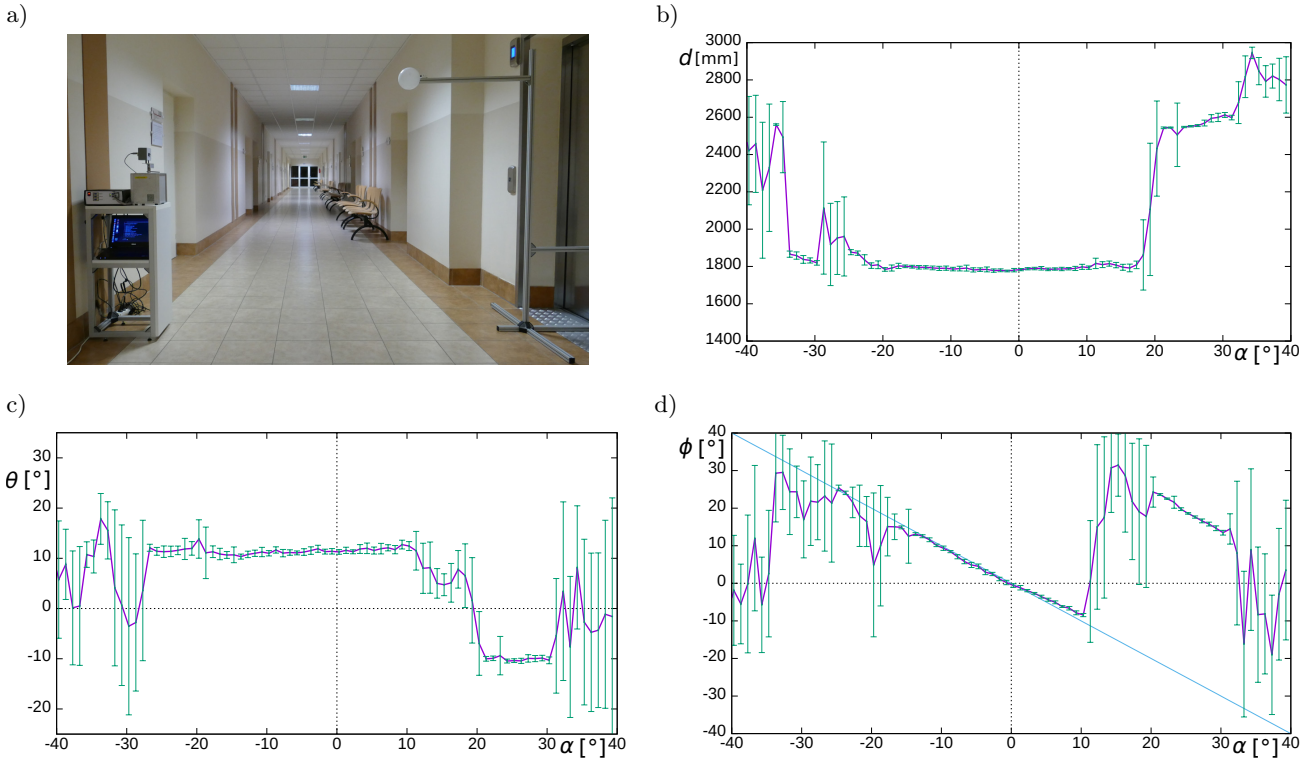

Fig. 15. Results of measurements performed for the glass ball depending on the orientation angle α of the sonar module. The glass ball was placed above the horizontal plane of the sonar module: a) arrangement of the sonar stand and the glass ball; b) values of the measured distance d; c) determined values of the elevation angle θ; d) determined values of the azimuth angle ϕ.

higher RMSD values. In this case, the differences between the RMSD for the azimuth and elevation angles become much more apparent and significant. In the range of α $[-15°, 10°]$, the azimuth angle values are as expected. In the same range, the results of determining the elevation angle change very little. This is also as expected. Unfortunately, its values are below the desired one which is 16° while the obtained results are in the range $[11°, 13°]$. The main reason for this discrepancy is the small distance of the receivers in the vertical direction compared to their size. Due to the large diameter of the receivers in relation to their mutual distances, it can be assumed that treating them as fixed points is not sufficient for different angles of incidence of the acoustic wave. With small mutual vertical distances, even small changes in the location of these points translate into significant discrepancies in the determined angle. This makes it difficult to obtain uniform calibration parameters for the entire range of angles considered in this experiment.

In the next series of measurements, the glass ball was placed near the horizontal plane of the sonar module (see Fig. 16a). The elevation angle was about 1°. The object was detected in almost the entire range of orientation angles of the sonar module (see Fig. 16b). However, azimuth and elevation angle values, that were close to expected ones, were obtained only for the orientation range $[-20°, 19°]$ (see Figs. 16c and 16d).

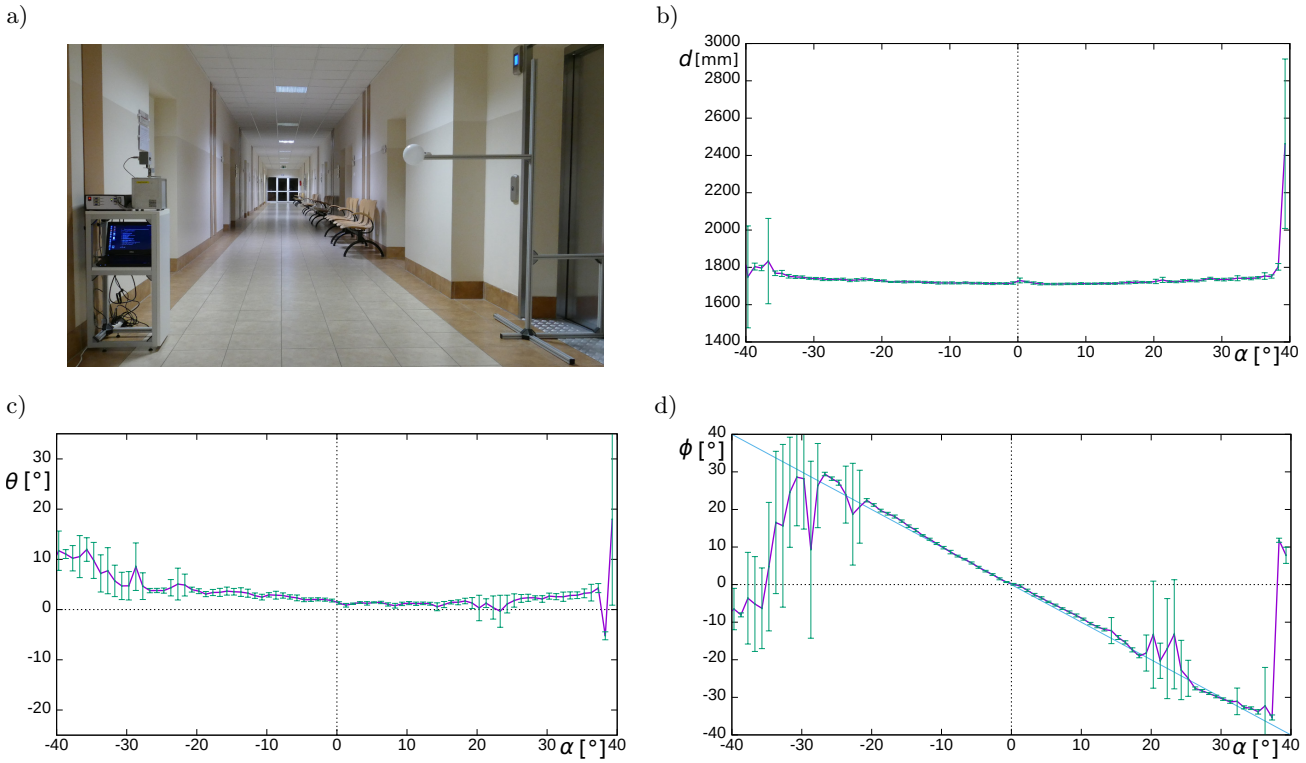

Fig. 16. Results of measurements performed for the glass ball depending on the orientation angle α of the sonar module. The glass ball was placed near the horizontal plane of the sonar module: a) arrangement of the sonar stand and the glass ball; b) values of the measured distance d; c) determined values of the elevation angle θ; d) determined values of the azimuth angle ϕ.

Compared to the previous case, a shift to the left of such an interval can be observed. This can be said even considering the much more limited visibility of the glass ball in the previous case. This is consistent with simulation results presented in Sec. 7 (see Fig. 8). In order to make it clearer and easier to interpret, the diagram shown in Fig. 8b should be presented in the space of the rotation angle α (orientation of the sonar module), instead of the azimuth angle ϕ. To do this, the relationship expressed by Eq. (15) must be taken into account. It flips the original diagram along the vertical axis (see Fig. 17a). The final form obtained after sonar calibration with marked lines relating to the results of the three experiments presented is shown in Fig. 17b. This offset is more evident in the results of the third experiment, when the glass ball was placed below the horizontal plane of the sonar module (see Fig. 18). The range of module orientations, for which

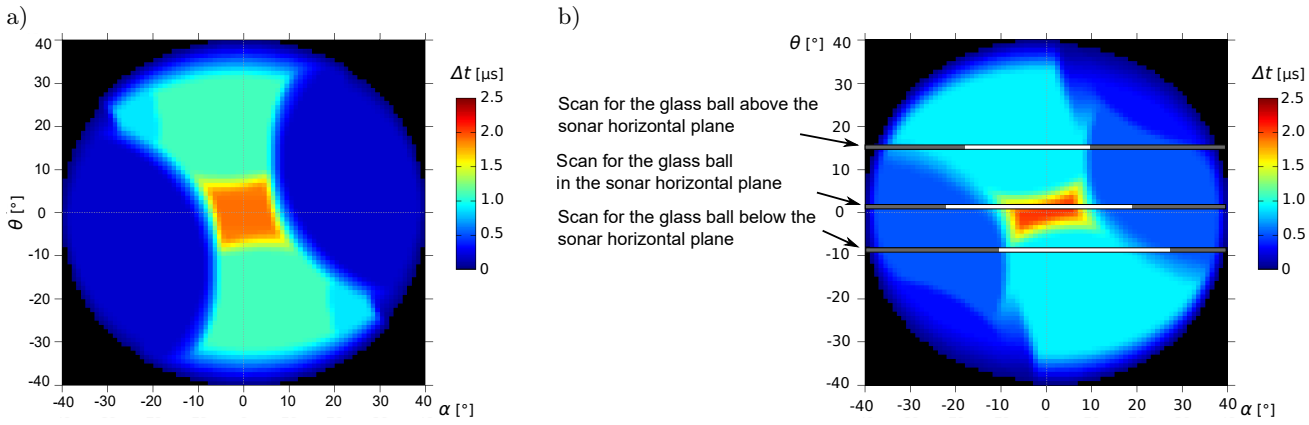

Fig. 17. Distribution of the maximal tolerable error of time measurement (top view) in space of the sonar module rotation angle α: a) for the arrangement of receivers in accordance with the original design; b) for the acoustic center coordinates of the receivers obtained after sonar calibration. The diagram also shows the lines corresponding to DOAs of the signals reflected by the glass sphere during the three consecutive experiments conducted. The white stripes represent regions where the determined DOAs were close to the expected values.

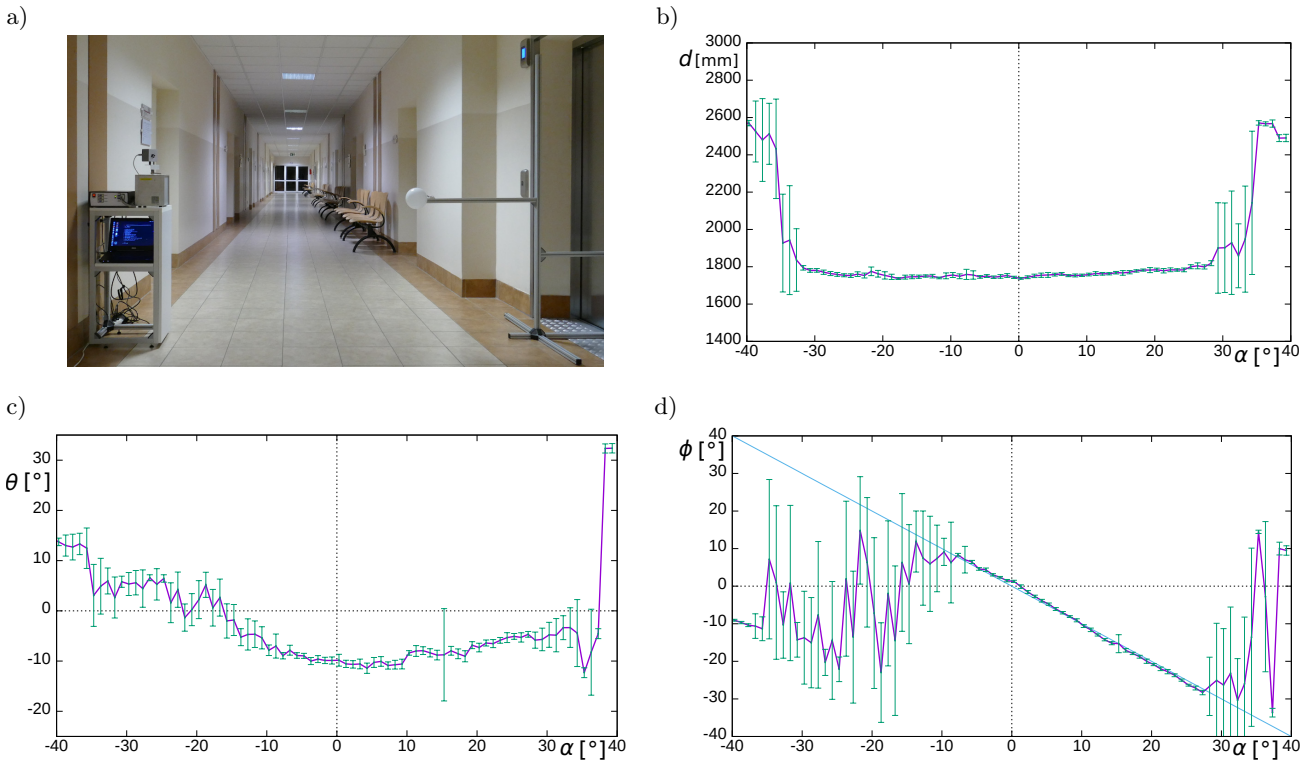

Fig. 18. Results of measurements performed for the glass ball depending on the orientation angle α of the sonar module. The glass ball was placed below the horizontal plane of the sonar module: a) arrangement of the sonar stand and the glass ball; b) values of the measured distance d; c) determined values of the elevation angle θ; d) determined values of the azimuth angle ϕ.

the azimuth angle was correctly determined, is shifted to $[-10°, 28°]$. Considering the elevation angle, larger deviations from the expected value (about 9°) are noticeable. It can be assumed that these disturbances result from the scattering of the returning ultrasonic wave at the upper edge of the base of the rotating sonar column (see Fig. 18a).

The simulation results presented in Fig. 17b take into account the correction of the position of the acoustic centers of the receivers obtained as a result of the calibration procedure. However, they do not take into account the directional patterns of the transmitter and receivers. Therefore, full agreement with experimental results cannot be expected. Nevertheless, the main trend of change is clearly visible. For the case of the wall shown in Fig. 13, this feature was not observed, as the received echoes were strong enough to cause very small measurement errors.

10. Conclusion and further research

The main advantage of the proposed method is its simplicity. However, the cost of simplicity is sensitivity to signal interference. Fortunately, the method makes it possible to distinguish the echo coming from a single object from overlapping echoes, and to assess the reliability of the results obtained (Kreczmer, 2021). The sonar module used in the experiments to verify the proposed method uses popular piezoelectric ultrasonic receivers. Due to their large size relative to their mutual distances, high accuracy DOA determination cannot be expected for a wide range of sonar module orientations. Nevertheless, in the case of a relatively strong echo received after reflecting the signal from objects such as a wall, the sonar module used works very well. The same cannot be said of the glass ball case. It is worth noting, however, that the observed limits of the sonar module orientation, for which acceptable results are obtained, are consistent with the simulation results. These limits are determined by the geometry of the receiver arrangement. The results of simulations and experiments also indicate that it is desirable to enlarge the distance between some receivers in order to increase the precision of angle determination. This can be clearly seen in the difference in the horizontal and vertical geometric arrangement of the receivers of the sonar module used. Due to this arrangement, the accuracy of the determined azimuth angle was greater than that of the elevation angle. To be able to determine azimuth and elevation angles with the same high accuracy, it is necessary to maintain an increased distance between the selected microphones in both horizontal and vertical directions. Another important consideration is to maximize in terms of angle and distance the

area visible by the sonar, for which the greatest possible robustness to measurement errors will be obtained. It seems that this feature is rather difficult to achieve with piezoelectric microphones. MEMS microphones are much more useful for this case. Furthermore, 4 microphones seem insufficient to achieve improvements in DOA determination accuracy. How much their number should be changed and how to arrange them is a topic for further research.

References

1. Allevato G., Rutsch M., Hinrichs J., Pesavento M., Kupnik M. (2020), Embedded air-coupled ultrasonic 3D sonar system with GPU acceleration, [in:] *2020 IEEE SENSORS*, pp. 1–4, doi: 10.1109/SENSORS47125.2020.9278601.
2. Barabell A. (1983), Improving the resolution performance of eigenstructure-based direction-finding algorithms, [in:] *ICASSP'83. IEEE International Conference on Acoustics, Speech, and Signal Processing*, pp. 336–339, doi: 10.1109/ICASSP.1983.1172124.
3. Cadzow J.A. (1990), Multiple source location the signal subspace approach, *IEEE Transactions on Acoustics, Speech, and Signal Processing*, **38**(7): 1110–1125, doi: 10.1109/29.57540.
4. Chen H., Ballal T., Muquaibel A.H., Zhang X., Al-Naffouri T.Y. (2020), Air writing via receiver array-based ultrasonic source localization, *IEEE Transactions on Instrumentation and Measurement*, **69**(10): 8088–8101, doi: 10.1109/TIM.2020.2991573.
5. Choi K.H., Ra W.-S., Park S.-Y., Park J.B. (2014), Robust least squares approach to passive target localization using ultrasonic receiver array, *IEEE Transactions on Industrial Electronics*, **61**(4): 1993–2002, doi: 10.1109/TIE.2013.2266076.
6. Cholewiński M., Dziergwa M., Kaczmarek P.M., Kędzierski J., Wnuk M. (2013), *Malaga minimodule* [in Polish], Technical report SPR no 13/2013, Wrocław University of Science and Technology.
7. Dokmanić I., Tashev I. (2014), Hardware and algorithms for ultrasonic depth imaging, [in:] *2014 IEEE International Conference on Acoustics, Speech and Signal Processing (ICASSP)*, pp. 6702–6706, doi: 10.1109/ICASSP.2014.6854897.
8. Gialich M., Im A., Lee T., Aliyazicioglu Z., Hwang H.K. (2012), DOA estimation using array antenna with large inter-element spacing, [in:] *2012 11th International Conference on Signal Processing (ICSP)*, pp. 1701–1704, doi: 10.1109/ICoSP.2012.6491908.
9. Haardt M., Nossek J.A. (1995), Unitary ESPRIT: How to obtain increased estimation accuracy with a reduced computational burden, *IEEE Transactions on Signal Processing*, **43**(5): 1232–1242, doi: 10.1109/78.382406.
10. Kapoor R., Ramasamy S., Gardi A., Schyndel R.V., Sabatini R. (2018), Acoustic sensors for air and surface navigation applications, *Sensors*, **18**(2): 499, doi: 10.3390/s18020499.
11. Kerstens R., Laurijssen D., Steckel J. (2017), Low-cost one-bit MEMS microphone arrays for in-air acoustic imaging using FPGA's, [in:] *2017 IEEE SENSORS*, pp. 1–3, doi: 10.1109/ICSENS.2017.8234087.
12. Kerstens R., Laurijssen D., Steckel J. (2019), eRTIS: A fully embedded real time 3D imaging sonar sensor for robotic applications, [in:] *2019 International Conference on Robotics and Automation (ICRA)*, pp. 1438–1443, doi: 10.1109/ICRA.2019.8794419.
13. Kleeman L. (1995), A three dimensional localiser for autonomous robot vehicles, *Robotica*, **13**(1): 87–94, doi: 10.1017/S0263574700017513.
14. Kreczmer B. (2018), Azimuth angle estimation of ultrasonic signal arrival by using multi-pair receiver system, [in:] *Automation 2018. Advances in Intelligent Systems and Computing*, Szewczyk R., Zieliński C., Kaliczyńska M. [Eds.], **743**: 672–681, doi: 10.1007/978-3-319-77179-3_65.
15. Kreczmer B. (2019), Estimation of the azimuth angle of the arrival direction for an ultrasonic signal by using indirect determination of the phase shift, *Archives of Acoustics*, **44**(3): 585–601, doi: 10.24425/aoa.2019.129273.
16. Kreczmer B. (2021), Influence of signal interference on determining direction of arrival by using the indirect phase determination method, [in:] *Automation 2021: Recent Achievements in Automation, Robotics and Measurement Techniques. AUTOMATION 2021. Advances in Intelligent Systems and Computing*, Szewczyk R., Zieliński C., Kaliczyńska M. [Eds.], Springer International Publishing, pp. 319–328, doi: 10.1007/978-3-030-74893-7_30.
17. Krim H., Viberg M. (1996), Two decades of array signal processing research: The parametric approach, *IEEE Signal Processing Magazine*, **13**(4): 67–94, doi: 10.1109/79.526899.
18. Krishnaveni V., Kesavamurthy T., Aparna B. (2013), Beamforming for direction-of-arrival (DOA) estimation – A survey, *International Journal of Computer Applications*, **61**(11): 4–11, doi: 10.5120/9970-4758.
19. Li P., Li C., Ye C., Zhang X. (2020), Low complexity DOA estimation using coprime circular array, [in:] *2020 IEEE 5th International Conference on Signal and Image Processing (ICSIP)*, pp. 592–597, doi: 10.1109/ICSIP49896.2020.9339298.
20. Peremans H., Audenaert K., Van Campenhout J.M. (1993), A high-resolution sensor based on tri-aural perception, *IEEE Transactions on Robotics and Automation*, **9**(1): 36–48, doi: 10.1109/70.210793.
21. Roy R., Kailath T. (1989), ESPRIT estimation of signal parameters via rotational invariance techniques, *IEEE Transactions on Acoustics, Speech, and Signal Processing*, **37**(7): 984–995, doi: 10.1109/29.32276.
22. Roy R., Paulraj A., Kailath T. (1986), Direction-of-arrival estimation by subspace rotation methods – ESPRIT, [in:] *ICASSP '86. IEEE International Conference on Acoustics, Speech, and Signal Processing*, pp. 2495–2498, doi: 10.1109/ICASSP.1986.1168673.

23. Schmidt R. (1986), Multiple emitter location and signal parameter estimation, *IEEE Transactions on Antennas and Propagation*, **34**(3): 276–280, doi: 10.1109/TAP.1986.1143830.

24. Steckel J., Boen A., Peremans H. (2013), Broadband 3-D sonar system using a sparse array for indoor navigation, robotics, *IEEE Transactions on Robotics*, **29**(1): 161–171, doi: 10.1109/TRO.2012.2221313.

25. Sun F., Lan P., Gao B. (2015), Partial spectral search-based DOA estimation method for co-prime linear arrays, *Electronics Letters*, **51**(24): 2053–2055, doi: 10.1049/el.2015.2261.

26. Tayem N., Kwon H.M. (2003), Conjugate ESPRIT (C-SPRIT), [in:] *Proceedings of IEEE Military Communications Conference, 2003, MILCOM 2003*, pp. 1155–1160, doi: 10.1109/MILCOM.2003.1290358.

27. Van Trees H.L. (2004), Optimum Array Processing: Part IV of Detection, Estimation, and Modulation Theory Detection, Estimation, and Modulation Theory, John Wiley & Sons, Inc.

28. Van Veen B.D., Buckley K.M. (1988), Beamforming: A versatile approach to spatial filtering, *IEEE ASSP Magazine*, **5**(2): 4–24, doi: 10.1109/53.665.

29. Verellen T., Kerstens R., Steckel J. (2020), High-resolution ultrasound sensing for robotics using dense microphone arrays, [in:] *IEEE Access*, **8**: 190083–190093, doi: 10.1109/ACCESS.2020.3032177.

30. Yang X., Wu X., Li S., Sarkar T.K. (2018), A fast and robust DOA estimation method based on JSVD for co-prime array, [in:] *IEEE Access*, **6**: 41697–41705, doi: 10.1109/ACCESS.2018.2860680.

31. Zhou C., Shi Z., Gu Y., Shen X. (2013), DECOM: DOA estimation with combined MUSIC for coprime array, [in:] *2013 International Conference on Wireless Communications and Signal Processing*, pp. 1–5, doi: 10.1109/WCSP.2013.6677080.